

# Effect of thermomechanical treatment on structure and properties of metastable Ti-25Nb-8Sn alloy

H.-C. Hsu<sup>1</sup>, K.-K. Wong<sup>2</sup>, J.-S. Chen<sup>2</sup>, S.-C. Wu<sup>1</sup>, W.-F. Ho<sup>2\*</sup>

<sup>1</sup>Department of Dental Technology and Materials Science, Central Taiwan University of Science and Technology, Taichung 40601, Taiwan

<sup>2</sup>Department of Chemical and Materials Engineering, National University of Kaohsiung, Kaohsiung 81148, Taiwan

Received 9 July 2021, received in revised form 12 October 2021, accepted 20 October 2021

## Abstract

In this work, different thermomechanical treatment conditions were used to improve the mechanical performances of Ti-25Nb-8Sn. During cold rolling treatment (50, 75, and 90 %), as-cast Ti-25Nb-8Sn underwent a stress-induced phase transformation from a single  $\beta$  phase to a three-phase structure of  $\alpha'' + \beta + \omega_{\text{str}}$ . After the subsequent aging treatment, Ti-25Nb-8Sn presents three-phase  $\beta + \alpha'' + \omega_{\text{iso}}$  (at 250 and 400 °C, for 30 min) and two-phase  $\beta + \alpha$  (at 600 °C, for 30 min). At lower aging temperatures (250 and 400 °C), yield strength/modulus ( $\times 1000$ ) ratios of Ti-25Nb-8Sn are dramatically improved with a maximum increase of 143 %, from 9.06 (as-cast) to 16.2–22.0. Under various thermomechanical treatment conditions in this study, the results show that Ti-25Nb-8Sn has excellent yield strength/modulus ( $\times 1000$ ) ratio ( $\sim 22$ ) and corrosion resistance after 90 % cold rolling and subsequent aging treatment at 250 and 400 °C for 30 min.

Key words: titanium alloys, biomaterials, cold working, aging, hardness

## 1. Introduction

Commercial pure titanium (c.p. Ti) and Ti-6Al-4V have an excellent specific strength, corrosion resistance, and biocompatibility and are often used as medical implant materials [1]. Biomedical implants are required to have good biocompatibility and corrosion resistance, but low elastic modulus is another important indicator. When the implant is much stiffer than bone tissue, it can cause the stress shielding effect [2, 3]. Although the elastic modulus (110 GPa) of Ti-6Al-4V alloy is much lower than those of 316L stainless steel (205 GPa) and Co-Cr-Mo alloy (230 GPa) [1], it is still several times higher than that of human cortical bone (10–30 GPa). In addition, Ti-6Al-4V contains aluminum (Al) and vanadium (V) that are harmful to the human body [4, 5]. In recent years, many  $\beta$ -type Ti alloys with low elastic modulus and without Al and V elements have been widely developed, such as Ti-5Nb-5Mo [6, 7], Ti-26Zr-24Nb [8], Ti-Nb-Zr-Fe-O [9], Ti-Nb-Ta-O [10], Ti-20Nb-5Ag [11], and Ti-4Fe [12]. Ti-Nb-Sn alloys have been proven to have

good corrosion resistance [13] and bone histocompatibility [14]. Adding more Nb elements can reduce the elastic modulus of Ti alloy [15], while adding Sn elements can effectively suppress the formation of the  $\omega$  phase [16, 17]. In our previous work [18], Ti-25Nb-8Sn with low elastic modulus (52 GPa) has been proposed. However, Ti alloys with low elastic modulus generally exhibit lower strength [19]. Enhancing the strength of Ti alloys can help improve their fatigue strength [20, 21], and increasing the hardness values of Ti alloys is also beneficial for the wear resistance [22].

Thermomechanical treatment (TMT) has attracted attention as an effective process to improve the mechanical performances of Ti alloys. The first stage of TMT is to deform the alloy (rolling or forging), which can achieve the effects of strain hardening and grain refinement [23], and then improve the strength of the material [24–26]. It is worth noting that the  $\beta$ -type Ti alloy with low phase stability (meta-stable  $\beta$ -type Ti alloy) would produce the stress-induced martensitic transformation ( $\beta \rightarrow \alpha''$ ) during the deformation process, which can reduce the elastic modulus of the

\*Corresponding author: tel.: +886-7-591-9276; fax: +886-7-591-9277; e-mail address: [fujii@nuk.edu.tw](mailto:fujii@nuk.edu.tw)

alloy [24]. Xie et al. [27] indicated that the grain size of Ti-36Nb-2.2Ta-3.7Zr-0.3O (at.%) decreased from 2  $\mu\text{m}$  to 10 nm after cold rolling treatment. As the grain size decreases, the elastic modulus of the alloy decreases significantly from 65 to 43 GPa, and the hardness of the alloy increases from 260 to 320 HV. Nunes et al. [28] reported that with the percentage of cold rolling up to 90 %, the hardness of Ti-29Nb-2Mo-6Zr increased from 228 to 278 HV, and its elastic modulus decreased from 93 GPa to 76 GPa. Also, they found that a greater amount of  $\alpha''$  phase in Ti-29Nb-2Mo-6Zr was induced with increasing cold-rolling percentage.

Aging treatment is the second stage of TMT, which can further enhance the strength of Ti alloys through precipitation strengthening. After TMT, metastable  $\beta$ -type Ti alloy may precipitate  $\alpha$  and/or  $\omega_{\text{iso}}$  phase [29, 30]. However, the  $\alpha$  and/or  $\omega_{\text{iso}}$  phase of precipitates may significantly increase the elastic modulus of the alloy [29–33]. The grain size, distribution, and volume fraction of precipitates in Ti alloys would significantly impact the mechanical properties of Ti alloys [34]. Therefore, it is essential to control the heat-treatment conditions of the aging process.

In this study, Ti-25Nb-8Sn was subjected to cold rolling and aging treatment under various conditions to achieve an excellent combination of high yield strength and low elastic modulus. The stress-induced phase transformation during the cold rolling process is expected to reduce the modulus of the alloy, and the precipitates generated by aging treatment are expected to improve the mechanical strength of the alloy. The phase transformation, microstructure, and mechanical properties of Ti-25Nb-8Sn under different cold rolling percentages (50, 75, and 90 %) and aging treatment (aging temperature: 250, 400, and 650 °C; aging time: 30 min) are discussed in this study.

## 2. Materials and methods

Ingots of the Ti-25Nb-8Sn were prepared from Ti (99.7 wt.% pure), Nb (99.95 wt.% pure), and Sn (99.9 wt.% pure) by using a commercial arc-melting vacuum pressure casting system (A-028, Dawn Shine, Taiwan). Before casting, the ingots were re-melted and flipped six times for chemical homogenization of constituent elements. After casting in a graphite mold, the rectangular Ti-25Nb-8Sn specimens were cold-rolled several times in the same direction with a double rolling machine (Jong Yih Electric Technology Co., Ltd., Taiwan) at different cold-rolling reduction ratios of 50 % (CR50), 75 % (CR75), and 90 % (CR90). The aging treatment of the cold-rolled samples was carried out by using a tubular high-temperature furnace (MTF 12/38/250, Carbolite Gero, UK) at 250 °C (A250), 400 °C (A400), and 650 °C (A650) for 30 min

Table 1. The nominal and actual compositions of Ti-25Nb-8Sn alloy obtained through SEM/EDS

Composition	Ti	Nb	Sn
Nominal	Bal.	25	8
Actual	Bal.	24.60 $\pm$ 0.24	7.77 $\pm$ 0.33

under argon atmosphere, and then quenched in ice water. The aging treatment was carried out after the tube furnace was preheated to the predetermined temperature. The  $\beta$  transus temperature of Ti-25Nb-8Sn was approximately 660 °C based on the Ti-Nb phase diagram [35].

The surfaces of all samples were ground using silicon carbide papers (#100 to #2000) and mechanically polished with colloidal 0.06  $\mu\text{m}$  SiO<sub>2</sub> suspension. After cleaning the surfaces of the samples with alcohol, acetone, and deionized water, respectively, using an ultrasonic cleaner (DC300, Delta, Taiwan), the alloys were etched in a solution of deionized water, nitric acid, and hydrofluoric acid at a volume ratio of 78:16:6. The microstructures of various processed alloys were examined using optical microscopy (OM; GmbH37081, Zeiss, Germany). The chemical composition of the Ti-25Nb-8Sn was obtained through scanning electron microscopy (SEM; 6330, JEOL, Japan), energy-dispersive X-ray spectroscopy (EDS). The nominal and actual compositions of the Ti-25Nb-8Sn alloy are displayed in Table 1. X-ray diffraction (XRD; D8-Advance, Bruker, Germany) analyses, microhardness measurements, three-point bending tests, and potentiodynamic polarization tests were performed on the polished samples. XRD patterns were used for phase analyses under Cu-K $\alpha$  radiation at 40 kV, 40 mA, a scanning speed of 4° min<sup>-1</sup>, a step size of 0.02°/step, and  $2\theta = 30^\circ$ – $80^\circ$ . The phase volume fractions of the alloy were calculated through the software (Origin-Pro 9, OriginLab Corporation, USA) from the integrated areas of the X-ray diffraction peaks [36]. Microhardness tests were measured by a Vickers hardness tester (MVK-E36, Mitutoyo, Japan). The load and dwelling time for the microhardness tests were 0.98 N and 15 s, respectively. Three-point bending tests were performed using a desktop mechanical tester (HT-2102AP, Hung-Ta Instrument, Taiwan), and the details are referred to the previous work by Wong et al. [37].

Potentiodynamic polarization tests were evaluated by the potentiostat (PGSTAT12, Autolab, Netherlands). The tests were conducted in Hanks' solution [38, 39], which was used as a simulating body fluid at room temperature (37 °C) and pH 7.4. The alloy sample, saturated calomel electrode (SCE), and platinum plate were used as the work electrode, reference electrode, and auxiliary electrode. Before start-

Table 2. Phases and phase volume fractions of Ti-25Nb-8Sn at various TMT conditions

Conditions	Phases	$V_{\beta}$ (%)	$V_{\alpha'}$ (%)	$V_{\omega_{str}}$ (%)	$V_{\omega_{iso}}$ (%)	$V_{\alpha}$ (%)
As cast	$\beta$	100	–	–	–	–
CR50	$\beta + \alpha'' + \omega_{str}$	58	36	6	–	–
CR50A250	$\beta + \alpha'' + \omega_{iso}$	57	35	–	8	–
CR50A400	$\beta + \alpha'' + \omega_{iso}$	65	24	–	11	–
CR50A650	$\beta + \alpha$	80	–	–	–	20
CR75	$\beta + \alpha'' + \omega_{str}$	49	44	7	–	–
CR75A250	$\beta + \alpha'' + \omega_{iso}$	63	32	–	5	–
CR75A400	$\beta + \alpha'' + \omega_{iso}$	67	26	–	7	–
CR75A650	$\beta + \alpha$	92	–	–	–	8
CR90	$\beta + \alpha'' + \omega_{str}$	68	27	5	–	–
CR90A250	$\beta + \alpha'' + \omega_{iso}$	67	28	–	5	–
CR90A400	$\beta + \alpha'' + \omega_{iso}$	71	22	–	7	–
CR90A650	$\beta + \alpha$	83	–	–	–	17

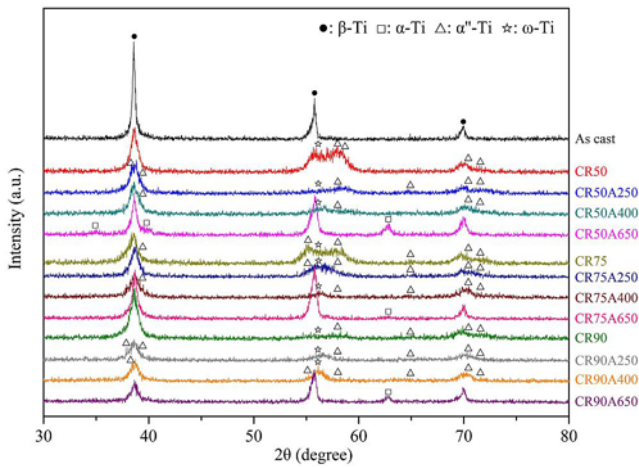


Fig. 1. XRD patterns of Ti-25Nb-8Sn alloys at various TMT conditions.

ing the test, the electrolyte solution was deoxygenized using nitrogen gas for 30 min. Afterward, the sample was soaked in Hanks' solution for an hour to stabilize the open circuit potential (OCP). The scan rate and scan range were  $1 \text{ mV s}^{-1}$  and  $-2.0$  to  $2.0 \text{ V}$ , respectively. The Hank's solution was comprised of  $\text{NaCl}$  ( $8.035 \text{ g L}^{-1}$ ),  $\text{NaHCO}_3$  ( $0.355 \text{ g L}^{-1}$ ),  $\text{KCl}$  ( $0.225 \text{ g L}^{-1}$ ),  $\text{K}_2\text{HPO}_4 \cdot 3\text{H}_2\text{O}$  ( $0.231 \text{ g L}^{-1}$ ),  $\text{MgCl}_2 \cdot 6\text{H}_2\text{O}$  ( $0.311 \text{ g L}^{-1}$ ),  $1 \text{ M HCl}$  ( $39 \text{ mL}$ ),  $\text{CaCl}_2$  ( $0.292 \text{ g L}^{-1}$ ),  $\text{Na}_2\text{SO}_4$  ( $0.072 \text{ g L}^{-1}$ ), and  $(\text{CH}_2\text{OH})_3\text{CNH}_2$  ( $6.118 \text{ g L}^{-1}$ ).

### 3. Results and discussion

#### 3.1. Phase structure

The XRD patterns of Ti-25Nb-8Sn alloy under different processing conditions are shown in Fig. 1. As-cast Ti-25Nb-8Sn presents a single  $\beta$  phase. Both Nb

and Sn are  $\beta$ -stabilizing elements [15], and the presence of Sn can inhibit the formation of the  $\omega$  phase [16, 17]. After 50, 75, and 90% cold rolling, the alloy shows a three-phase structure of  $\alpha'' + \beta + \omega_{str}$ . The generation of  $\alpha''$  and  $\omega_{str}$  was related to the stress-induced transformation ( $\beta \rightarrow \alpha'' + \omega_{str}$ ) [24, 40–43]. The phases and phase volume fractions of alloys under various processing conditions are listed in Table 2. For CR50, CR75, and CR90, the volume fractions of  $\alpha''$  are 36, 44, and 27%, respectively. The volume fraction of  $\alpha''$  in CR75 was significantly greater than that of CR50, but CR90 presents the smallest volume fraction of  $\alpha''$ . Although a higher cold rolling reduction produces more  $\alpha''$ , excessive grain refinement and dislocations caused by severe plastic deformation in CR90 would inhibit the stress-induced martensitic transformation [44].

After aging treatment at different temperatures (250, 400, and  $650^\circ\text{C}$ ) for 30 min, it can be observed that the volume fraction of  $\alpha''$  decreases, which is attributed to the reverse phase transformation of  $\alpha''$  back to  $\beta$  during the heat treatment [45–47]. All the Ti-25Nb-8Sn aged at 250 and  $400^\circ\text{C}$  show  $\beta + \alpha'' + \text{isothermal } \omega$  ( $\omega_{iso}$ ) phase, and all the Ti-25Nb-8Sn aged at  $650^\circ\text{C}$  exhibit  $\beta + \alpha$  phase. The  $\omega_{iso}$  phase would generally precipitate in  $\beta$ -Ti alloys within the aging temperature range of 200 to  $500^\circ\text{C}$  [48–50]. The phase volume fractions of  $\omega_{iso}$  in CR90A250 and CR75A250 were lower than that of CR50A250, which is due to a large number of dislocations in the alloy after cold rolling hinder the phase transformation of  $\beta \rightarrow \omega_{iso}$  [44]. Furthermore, the  $\alpha$  phase would precipitate in  $\beta$ -Ti alloys at an aging temperature above  $500^\circ\text{C}$  [49].

#### 3.2. Microstructure

The metallographic images of Ti-25Nb-8Sn alloy under various TMT conditions are shown in Fig. 2. As-cast Ti-25Nb-8Sn presents a typical dendritic struc-

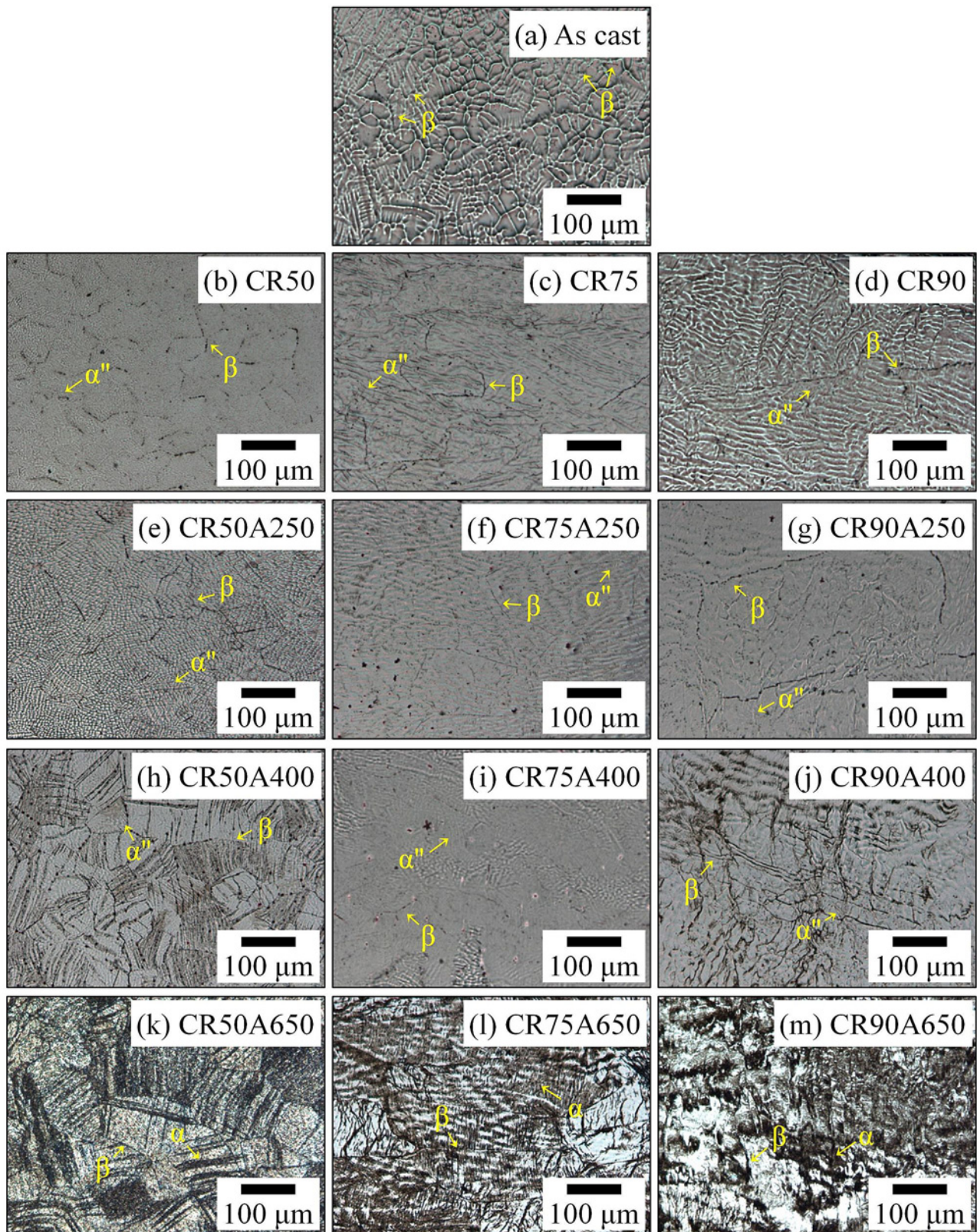


Fig. 2. Optical micrographs of Ti-25Nb-8Sn alloys at various TMT conditions: (a) as cast, (b)–(d) after cold rolling, and (e)–(m) after cold rolling and aging treatment.

ture and equiaxed  $\beta$  grains (Fig. 2a). After 50% cold rolling, a small amount of fine needle-like  $\alpha''$

structure appears in the metallograph of CR50, and the equiaxed  $\beta$  grains are retained (Fig. 2b). Simi-

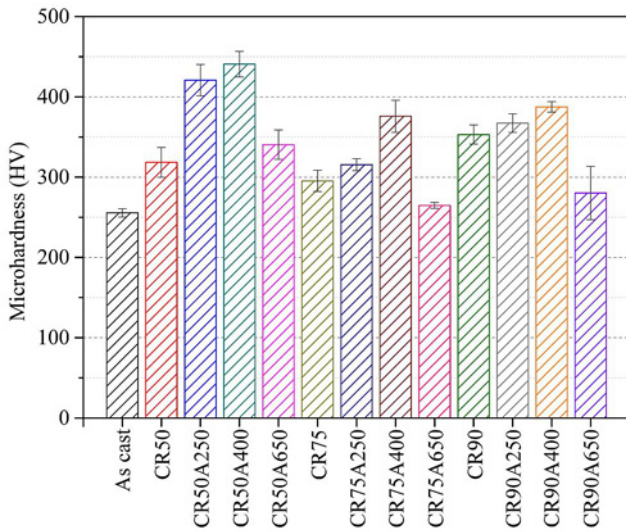


Fig. 3. Microhardness values of Ti-25Nb-8Sn at various TMT conditions.

larly, CR75 and CR90 also exhibit equiaxed  $\beta$  grains and a small amount of fine needle-like  $\alpha''$  structure (Figs. 2c,d). When the percentage of cold rolling reduction increased (75 and 90%), equiaxed  $\beta$  grains were gradually elongated along the cold rolling direction. However, the equiaxed  $\beta$  grains of CR50 were not significantly elongated, which may be attributed to a lower percentage of cold rolling [25]. In addition, since  $\omega_{\text{str}}$  is a nanoscale precipitate, the morphology of the  $\omega_{\text{str}}$  phase could not be observed in the metallographic images of CR50, CR75, and CR90 [41].

After aging at 250 or 400 °C, Ti-25Nb-8Sn shows  $\beta$  (equiaxed grains) +  $\alpha''$  (fine needle-like) +  $\omega_{\text{iso}}$  structure (Figs. 2e–j). As mentioned in the results of XRD, the aging treatment of  $\beta$ -Ti alloys in the range of 200 to 500 °C would tend to precipitate the  $\omega_{\text{iso}}$  [50]. In addition, due to insufficient aging time (30 min), the  $\alpha''$  martensitic phase was still observed in the Ti-25Nb-8Sn alloy after aging at 250 and 400 °C. When the aging treatment was performed at 650 °C, CR50A650, CR75A650, and CR90A600 exhibit  $\beta$  (equiaxed grains) +  $\alpha$  (plate-like), as shown in Figs. 2k–m.

### 3.3. Mechanical properties

The microhardness values of Ti-25Nb-8Sn under various TMT conditions are shown in Fig. 3. The hardness of as-cast Ti-25Nb-8Sn alloy is 255.6 HV. After 50, 75, and 90% cold rolling treatment, the hardness of the alloys increased to 318.4, 295.2, and 353 HV, respectively. The high dislocation density produced by cold rolling leads to a significant strain hardening or work hardening, which increases the hardness

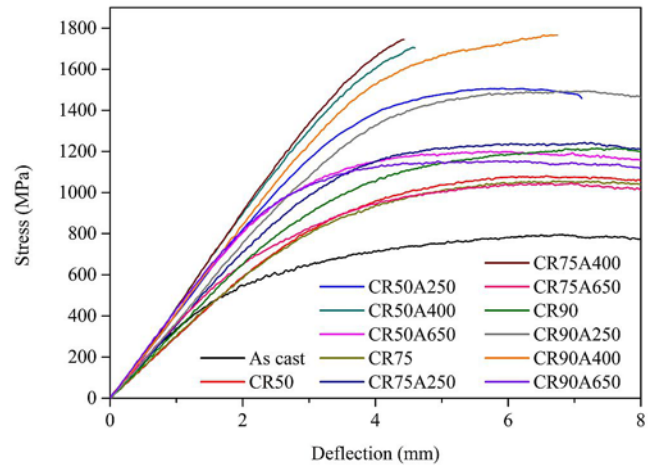


Fig. 4. Stress-deflection curves of Ti-25Nb-8Sn at various TMT conditions obtained through three-point bending tests.

of the alloy [51, 52]. Therefore, CR90, which has the highest amount of plastic deformation, has the highest hardness. However, the hardness value of CR75 is lower than that of CR50 because the volume fraction of the  $\alpha''$  phase in CR75 is greater than that of CR50. The hardness of the  $\alpha''$  phase with an orthorhombic structure is lower than that of the  $\beta$  phase with a body-centered cubic structure [53, 54]. Among all the aging-treated alloys, CR50A400 has the highest hardness (440.8 HV), attributed to the greatest volume fraction of the  $\omega_{\text{iso}}$  phase. Similarly, among all the aged alloys with a structure of  $\beta + \alpha'' + \omega_{\text{iso}}$ , CR75A250 with the lowest volume fraction of  $\omega_{\text{iso}}$  phase has the lowest hardness (315.5 HV). Therefore, both the volume fraction of the  $\omega_{\text{iso}}$  phase and strain hardening contributed to enhancing the hardness of the alloy. On the other hand, CR50A650, CR75A650, and CR90A650 with  $\beta + \alpha$  structure exhibit relatively lower hardness (340.3, 264.7, and 280.1 HV, respectively). Although the precipitation of fine  $\alpha$  phase can increase the hardness of the alloy, larger  $\alpha$  grains would reduce the area fraction of the  $\alpha/\beta$  phase boundary, resulting in a decrease in the hardness of the alloy [55, 56].

The stress-deflection curves of three-point bending tests for Ti-25Nb-8Sn under various TMT conditions are displayed in Fig. 4. CR50A400 and CR75A400 broke after slightly exceeding the yield point during the three-point bending test. It was attributed to the excessive volume fractions of the  $\omega_{\text{iso}}$  phase in the alloys that deteriorated the deformability of the alloy [57]. On the other hand, the bending deflections of CR50A250, CR75A250, CR90A250, and CR90A400 with lower volume fractions of  $\omega_{\text{iso}}$  phase were even greater than 6 mm, while CR75A250 and CR90A250 did not break during the bending test (exceeding the

Table 3. Mechanical properties of Ti-25Nb-8Sn at various TMT conditions obtained through three-point bending tests

Conditions	Bending strength (MPa)	Yield strength, $\sigma_y$ (MPa)	Elastic modulus, $E$ (GPa)	$\sigma_y/E$ ( $\times 1000$ )
As cast	1027	462	51	9.1
CR50	1133	795	49	16.2
CR50A250	1534	1193	67	17.4
CR50A400	1750	1469	73	20.1
CR50A650	1249	939	68	13.8
CR75	1113	724	47	15.4
CR75A250	1286	923	57	16.2
CR75A400	1789	1624	74	22.0
CR75A650	1090	660	56	11.8
CR90	1297	863	53	16.3
CR90A250	1546	1200	61	19.7
CR90A400	1816	1473	68	21.7
CR90A650	1196	926	66	14.0

preset bending deflection of 8 mm). Table 3 presents the bending strength, yield strength ( $\sigma_y$ ), and elastic modulus ( $E$ ) of Ti-25Nb-8Sn under various TMT conditions. CR90A400 with  $\beta + \alpha'' + \omega_{\text{iso}}$  structure exhibits the highest bending strength (1816 MPa), which is attributed to the strengthening effect from  $\omega_{\text{iso}}$  precipitates and strain strengthening by cold rolling [58]. CR75A400 shows the second highest bending strength (1789 MPa), and its yield strength (1624 MPa) is much higher than that of the other alloys. Unfortunately, CR75A400 has insufficient plastic deformation ability and fractures before reaching the maximum bending strength, making it difficult for further engineering applications. Similar to the results of hardness tests, the bending strengths and yield strengths of CR50A650, CR75A650, and CR90A650 with  $\beta + \alpha$  structure are lower than those of the other alloys with  $\beta + \alpha'' + \omega_{\text{iso}}$  structure.

The elastic modulus (51 GPa) of as-cast Ti-25Nb-8Sn alloy was changed to 49, 47, and 53 GPa after 50, 75, and 90 % cold rolling, respectively. CR75 has the lowest modulus than CR50 and CR90 because CR75 has the highest volume fraction of the martensitic  $\alpha''$  phase. The stress-induced martensitic transformation ( $\beta \rightarrow \alpha''$ ) caused by cold rolling directly leads to the decrease of the modulus of the alloy [24]. Furthermore, the  $\omega_{\text{str}}$  phase in CR50, CR75, and CR90 does not seem to significantly affect the elastic modulus of the alloy. On the other hand, CR75A250 has the lowest elastic modulus (56 GPa) among the alloys with  $\beta + \alpha'' + \omega_{\text{iso}}$  structure. It is worth noting that CR50A400 and CR75A400, with the highest amount of  $\omega_{\text{iso}}$ , exhibit the greatest elastic moduli (73 and 74 GPa, respectively). Therefore, compared to  $\omega_{\text{str}}$ , the volume fraction of  $\omega_{\text{iso}}$  in the alloy has a strong influence on the elastic modulus of the alloy.

Evaluating the mechanical property of an excellent implant requires consideration of both yield strength and elastic modulus. The high yield strength of an

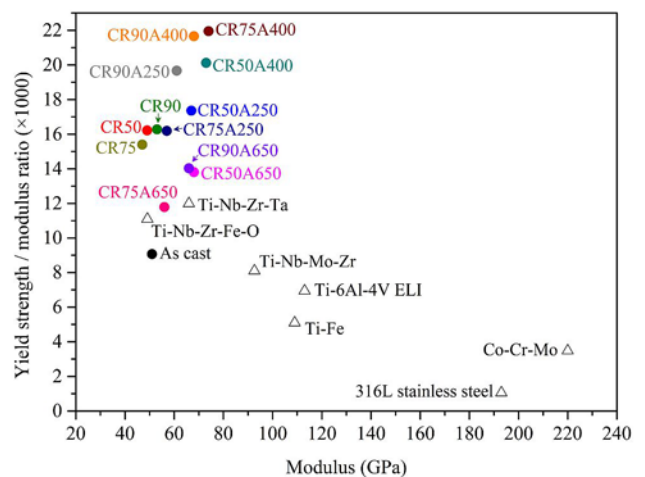


Fig. 5. Yield strength/elastic modulus ratios ( $\times 1000$ ) of Ti-25Nb-8Sn at various TMT conditions and various  $\beta$ -type Ti alloys [1, 9, 12, 28, 37].

implant can prevent its deformation or break in the human body environment [20, 21]. Furthermore, an implant with a low elastic modulus can avoid the stress shielding effect [2, 3].

The yield strength/modulus ( $\sigma_y/E$ )( $\times 1000$ ) ratios and moduli of Ti-25Nb-8Sn under various TMT conditions and various  $\beta$ -type Ti alloys [1, 9, 12, 28, 37] are shown in Fig. 5 and Table 3. The  $\sigma_y/E$  ( $\times 1000$ ) ratios of all Ti-25Nb-8Sn alloys under various conditions in this work (9.1–22.0) were significantly greater than those of Ti-6Al-4V (6.9), 316L stainless steel (1.1), and Co-Cr-Mo (3.5). Among them, CR75A400 has the greatest  $\sigma_y/E$  ( $\times 1000$ ) value (22.0). Furthermore, CR90A400, CR50A400, and CR90A250 with  $\beta + \alpha'' + \omega_{\text{iso}}$  have greater  $\sigma_y/E$  ( $\times 1000$ ) values, which are 21.7, 20.1, and 19.7, respectively. However, CR50A400 and CR75A400 exhibit insufficient plastic deformation ability in the three-point bending

Table 4. Corrosion potential ( $E_{\text{corr}}$ ), corrosion current density ( $I_{\text{corr}}$ ), passivation potential ( $E_{\text{pass}}$ ), and passivation current density ( $I_{\text{pass}}$ ) of Ti-25Nb-8Sn at various TMT conditions

Conditions	$E_{\text{corr}}$ (mV (v.s. SCE))	$I_{\text{corr}}$ ( $\mu\text{A cm}^{-2}$ )	$E_{\text{pass}}$ (mV (v.s. SCE))	$I_{\text{pass}}$ ( $\mu\text{A/cm}^{-2}$ )
As cast	-600.05	0.36	0.18	7.51
CR90	-633.06	49.60	-0.09	5020.00
CR90A250	-615.60	0.36	-0.02	5.45
CR90A400	-499.38	0.14	0.07	3.75

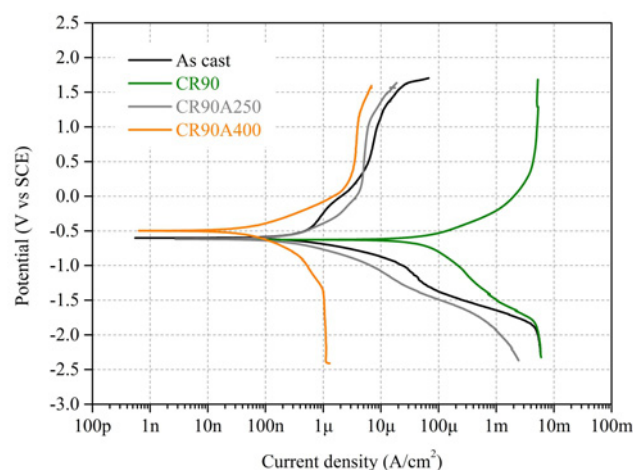


Fig. 6. Polarization curves of Ti-25Nb-8Sn at different processing conditions (as-cast Ti-25Nb-8Sn, CR90, CR90A250, and CR90A400) in Hank's solution at 37°C.

test, which was not conducive for practical applications. From the perspective of mechanical properties, CR90A250 and CR90A400 have great potential for use as biomedical implants.

### 3.4. Potentiodynamic polarization test

The polarization curves of as-cast Ti-25Nb-8Sn, CR90, CR90A250, and CR90A400 with the scan rate of  $1 \text{ mV s}^{-1}$  in Hank's solution at 37°C are shown in Fig. 6. According to the results presented in Fig. 6, the corrosion potential ( $E_{\text{corr}}$ ), corrosion current density ( $I_{\text{corr}}$ ), passivation potential ( $E_{\text{pass}}$ ), and passivation current density ( $I_{\text{pass}}$ ) of each alloy are shown in Table 4. The  $E_{\text{corr}}$  of as-cast Ti-25Nb-8Sn, CR90, CR90A250, and CR90A400 are all below 0 V. CR90A400 has the highest  $E_{\text{corr}}$  ( $-499.4 \text{ mV}$ ), and CR90 has the lowest  $E_{\text{corr}}$  ( $-633.1 \text{ mV}$ ). Similarly, CR90A400 has the lowest  $I_{\text{corr}}$  ( $0.14 \mu\text{A cm}^{-2}$ ) and  $I_{\text{pass}}$  ( $3.75 \mu\text{A cm}^{-2}$ ), while CR90 has the highest  $I_{\text{corr}}$  ( $49.6 \mu\text{A cm}^{-2}$ ) and  $I_{\text{pass}}$  ( $5020 \mu\text{A cm}^{-2}$ ). The corrosion resistance of CR90 is significantly lower than that of the other three alloys. Due to a large number of dislocations and grain boundaries in CR90, the corrosion

resistance of the alloy is reduced. Furthermore, the residual stress generated by cold rolling can also reduce the corrosion resistance of the alloy [59]. Aging treatment can effectively reduce the dislocation density, grain boundary area, and residual stress field of the alloy so that the corrosion resistance of CR90A250 and CR90A400 was much greater than that of CR90. Therefore, CR90A250 and CR90A400 exhibit better corrosion resistance and have good mechanical properties, which can meet the application requirements of biomedical implants.

## 4. Conclusions

In this study, the performance of as-cast Ti-25Nb-8Sn was improved by TMT (cold rolling: 50, 75, and 90 %; aging temperature: 250, 400, and 650 °C; aging time: 30 min). When cold rolling with 50, 75, and 90 % reduction, Ti-25Nb-8Sn with single  $\beta$  phase underwent a stress-induced phase transformation ( $\beta \rightarrow \alpha'' + \omega_{\text{str}}$ ), showing a three-phase structure of  $\alpha'' + \beta + \omega_{\text{str}}$ . After low-temperature aging treatment at 250 and 400 °C, all the alloys present  $\beta + \alpha'' + \omega_{\text{iso}}$  structure, while the alloys were transformed to two-phase  $\beta + \alpha$  structure after high-temperature aging treatment at 650 °C. The bending strength of Ti-25Nb-8Sn after TMT (1286–1816 MPa) was significantly higher than that of as-cast Ti-25Nb-8Sn (1027 MPa), which is attributed to the strengthening effect from  $\omega_{\text{iso}}$  precipitates and strain strengthening by cold rolling. Furthermore, the  $\sigma_y/E$  ( $\times 1000$ ) ratios of Ti-25Nb-8Sn after TMT (11.8–22.0) were significantly higher than those of as-cast Ti-25Nb-8Sn (9.1), Ti-6Al-4V (6.9), 316L stainless steel (1.1), and Co-Cr-Mo (3.5). Among them, CR90A250 and CR90A400 with  $\beta + \alpha'' + \omega_{\text{iso}}$  have greater  $\sigma_y/E$  ( $\times 1000$ ) values, 19.7 and 21.7, respectively. Moreover, the results of potentiodynamic polarization tests showed that both CR90A250 and CR90A400 have good corrosion resistance, exhibiting low  $I_{\text{pass}}$  ( $5.45$  and  $3.75 \mu\text{A cm}^{-2}$ , respectively) and low  $I_{\text{corr}}$  ( $0.36$  and  $0.14 \mu\text{A cm}^{-2}$ , respectively). Accordingly, CR90A250 and CR90A400 have extremely high  $\sigma_y/E$  ( $\times 1000$ ) ratios, good deformability, and better corrosion resistance, which have great potential for use as biomedical implants.

## Acknowledgement

The authors acknowledge the partial financial support of the National University of Kaohsiung.

## References

- [1] L. C. Zhang, L. Y. Chen, A review on biomedical titanium alloys: Recent progress and prospect, *Adv. Funct. Mater.* 21 (2019) 1801215. [doi:10.1002/adem.201801215](https://doi.org/10.1002/adem.201801215)
- [2] Q. Chen, G. A. Thouas, Metallic implant biomaterials, *Mater. Sci. Eng. R* 87 (2015) 1–57. [doi:10.1016/j.mser.2014.10.001](https://doi.org/10.1016/j.mser.2014.10.001)
- [3] K. T. Kang, Y. G. Koh, J. A. Lee, J. J. Lee, P. S. Kim, S. K. Kwon, The influence of the number of holes in the open wedge high tibial osteotomy on knee biomechanics using finite element analysis, *Orthop. Traumatol. Surg. Res.* 107 (2021) 102884. [doi:10.1016/j.otsr.2021.102884](https://doi.org/10.1016/j.otsr.2021.102884)
- [4] G. Khadija, A. Saleem, Z. Akhtar, Z. Naqvi, M. Gull, M. Masood, S. Mukhtar, M. Batool, N. Saleem, T. Rasheed, N. Nizam, A. Ibrahim, F. Iqbal, Short term exposure to titanium, aluminum and vanadium (Ti 6Al 4V) alloy powder drastically affects behavior and antioxidant metabolites in vital organs of male albino mice, *Toxicol. Rep.* 5 (2018) 765–770. [doi:10.1016/j.toxrep.2018.06.006](https://doi.org/10.1016/j.toxrep.2018.06.006)
- [5] P. Bocchetta, L. Y. Chen, J. D. C. Tardelli, A. C. Reis, F. Almeraya-Calderón, P. Leo, Passive layers and corrosion resistance of biomedical Ti-6Al-4V and  $\beta$ -Ti alloys, *Coatings* 11 (2021) 487. [doi:10.3390/coatings11050487](https://doi.org/10.3390/coatings11050487)
- [6] H. C. Hsu, S. C. Wu, S. K. Hsu, W. H. Kao, W. F. Ho, Structure and mechanical properties of as-cast Ti-5Nb-based alloy with Mo addition, *Mater. Sci. Eng. A* 579 (2013) 86–91. [doi:10.1016/j.msea.2013.05.004](https://doi.org/10.1016/j.msea.2013.05.004)
- [7] H. C. Hsu, S. C. Wu, Y. J. Su, W. F. Ho, Effects of thermal treatments on the microstructures and mechanical properties of Ti-5Nb-5Mo alloys, *Mater. Today Commun.* 26 (2021) 102059. [doi:10.1016/j.mtcomm.2021.102059](https://doi.org/10.1016/j.mtcomm.2021.102059)
- [8] F. L. Silva, L. M. Antonini, M. R. O. Vega, C. Aguzzoli, C. F. Malfatti, A new ternary alloy Ti<sub>26</sub>Zr<sub>24</sub>Nb for biomedical application: Behavior in corrosion, wear, and tribocorrosion, *J. Bio-Tribo-Corros.* 6 (2020) 86. [doi:10.1007/s40735-020-00376-5](https://doi.org/10.1007/s40735-020-00376-5)
- [9] V. D. Cojocar, A. Nocivin, C. Trisca-Rusu, A. Dan, R. Irimescu, D. Raducanu, B. M. Galbinas, Improving the mechanical properties of a  $\beta$ -type Ti-Nb-Zr-Fe-O alloy, *Metals* 10 (2020) 1491. [doi:10.3390/met10111491](https://doi.org/10.3390/met10111491)
- [10] S. Acharya, S. S. Dabas, S. Suwas, K. Chatterjee, Mechanical and electrochemical response in surface treated low modulus biomedical alloy Ti-Nb-Ta-O, *MATEC Web Conf.* 321 (2020) 05014. [doi:10.1051/mateconf/202032105014](https://doi.org/10.1051/mateconf/202032105014)
- [11] M. J. Shivaram, S. B. Arya, J. Nayak, B. B. Panigrahi, Tribocorrosion behaviour of biomedical porous Ti-20Nb-5Ag alloy in simulated body fluid, *J. Bio-Tribo-Corros.* 7 (2021) 59. [doi:10.1007/s40735-021-00491-x](https://doi.org/10.1007/s40735-021-00491-x)
- [12] J. Niu, Y. Guo, K. Li, W. Liu, Z. Dan, Z. Sun, H. Chang, L. Zhou, Improved mechanical, bio-corrosion properties and in vitro cell responses of Ti-Fe alloys as candidate dental implants, *Mater. Sci. Eng. C* 122 (2021) 111917. [doi:10.1016/j.msec.2021.111917](https://doi.org/10.1016/j.msec.2021.111917)
- [13] Y. F. Zheng, B. L. Wang, J. G. Wang, C. Li, L. C. Zhao, Corrosion behaviour of Ti-Nb-Sn shape memory alloys in different simulated body solutions, *Mater. Sci. Eng. A* 438–440 (2006) 891–895. [doi:10.1016/j.msea.2006.01.131](https://doi.org/10.1016/j.msea.2006.01.131)
- [14] N. Yamada, K. Miura, E. Itoi, S. Hanada, T. K. Jung, The bone tissue compatibility of a new Ti-Nb-Sn alloy with a low Young's modulus, *Acta Biomater.* 7 (2011) 2320–2326. [doi:10.1016/j.actbio.2011.02.008](https://doi.org/10.1016/j.actbio.2011.02.008)
- [15] C. M. Lee, C. P. Ju, J. H. Chern Lin, Structure-property relationship of cast Ti-Nb alloys, *J. Oral. Rehabil.* 29 (2002) 314–322. [doi:10.1046/j.1365-2842.2002.00825.x](https://doi.org/10.1046/j.1365-2842.2002.00825.x)
- [16] H. Matsumoto, S. Watanabe, S. Hanada, Microstructures and mechanical properties of metastable  $\beta$  TiNbSn alloys cold rolled and heat treated, *J. Alloy Compd.* 439 (2007) 146–155. [doi:10.1016/j.jallcom.2006.08.267](https://doi.org/10.1016/j.jallcom.2006.08.267)
- [17] Y. L. Hao, S. J. Li, S. Y. Sun, R. Yang, Effect of Zr and Sn on Young's modulus and superelasticity of Ti-Nb-based alloys, *Mater. Sci. Eng. A* 441 (2006) 112–118. [doi:10.1016/j.msea.2006.09.051](https://doi.org/10.1016/j.msea.2006.09.051)
- [18] H. C. Hsu, S. C. Wu, S. K. Hsu, J. Y. Syu, W. F. Ho, The structure and mechanical properties of as-cast Ti-25Nb- $x$ Sn alloys for biomedical applications, *Mater. Sci. Eng. A* 568 (2013) 1–7. [doi:10.1016/j.msea.2013.01.002](https://doi.org/10.1016/j.msea.2013.01.002)
- [19] M. Long, H. J. Rack, Titanium alloys in total joint replacement – a materials science perspective, *Biomaterials* 19 (1998) 1621–1639. [doi:10.1016/S0142-9612\(97\)00146-4](https://doi.org/10.1016/S0142-9612(97)00146-4)
- [20] J. C. Pang, S. X. Li, Z. G. Wang, Z. F. Zhang, General relation between tensile strength and fatigue strength of metallic materials, *Mater. Sci. Eng. A* 564 (2013) 331–341. [doi:10.1016/j.msea.2012.11.103](https://doi.org/10.1016/j.msea.2012.11.103)
- [21] J. C. Pang, S. X. Li, Z. G. Wang, Z. F. Zhang, Relations between fatigue strength and other mechanical properties of metallic materials, *Fatigue Fract. Eng. Mater. Struct.* 37 (2014) 958–976. [doi:10.1111/ffe.12158](https://doi.org/10.1111/ffe.12158)
- [22] M. G. Gee, A. Gant, B. Roebuck, Wear mechanisms in abrasion and erosion of WC/Co and related hard metals, *Wear* 263 (2007) 137–148. [doi:10.1016/j.wear.2006.12.046](https://doi.org/10.1016/j.wear.2006.12.046)
- [23] A. Zafari, X. S. Wei, W. Xu, K. Xia, Formation of nanocrystalline  $\beta$  structure in metastable  $\beta$  Ti alloy during high pressure torsion: the role played by stress induced martensitic transformation, *Acta Mater.* 97 (2015) 146–155. [doi:10.1016/j.actamat.2015.06.042](https://doi.org/10.1016/j.actamat.2015.06.042)
- [24] D. Kuczyńska-Zemła, E. Kijeńska-Gawrońska, A. Chlanda, A. Sotniczuk, M. Pisarek, K. Topolski, W. Swieszkowski, H. Garbacz, Biological properties of a novel  $\beta$ -Ti alloy with a low Young's modulus subjected to cold rolling, *Appl. Surf. Sci.* 511 (2020) 145523. [doi:10.1016/j.apsusc.2020.145523](https://doi.org/10.1016/j.apsusc.2020.145523)
- [25] S. Ozan, J. Lin, Y. Zhang, Y. Li, C. Wen, Cold rolling deformation and annealing behavior of a  $\beta$ -type Ti-34Nb-25Zr titanium alloy for biomedical applications, *J. Mater. Res. Technol.* 9 (2020) 2308–2318. [doi:10.1016/j.jmrt.2019.12.062](https://doi.org/10.1016/j.jmrt.2019.12.062)
- [26] Z. Du, Q. He, R. Chen, F. Liu, J. Zhang, F. Yang, X. Zhao, X. Cui, J. Cheng, Rolling reduction – dependent

- deformation mechanisms and tensile properties in a  $\beta$  titanium alloy, *J. Mater. Sci. Technol.* 104 (2021) 183–193. [doi:10.1016/j.jmst.2021.05.071](https://doi.org/10.1016/j.jmst.2021.05.071)
- [27] K. Y. Xie, Y. Wang, Y. Zhao, L. Chang, G. Wang, Z. Chen, Y. Cao, X. Liao, E. J. Lavernia, R. Z. Valiev, B. Sarrafpour, H. Zoellner, S. P. Ringer, Nanocrystalline  $\beta$ -Ti alloy with high hardness, low Young's modulus and excellent in vitro biocompatibility for biomedical applications, *Mater. Sci. Eng. C* 33 (2013) 3530–3536. [doi:10.1016/j.msec.2013.04.044](https://doi.org/10.1016/j.msec.2013.04.044)
- [28] A. R. V. Nunes, S. Borborema, L. S. Araújo, L. Malet, J. Dille, L. H. Almeida, Influence of thermo-mechanical processing on structure and mechanical properties of a new metastable  $\beta$  Ti-29Nb-2Mo-6Zr alloy with low Young's modulus, *J. Alloys Compd.* 820 (2020) 153078. [doi:10.1016/j.jallcom.2019.153078](https://doi.org/10.1016/j.jallcom.2019.153078)
- [29] M. T. Mohammed, Z. A. Khan, M. Geetha, A. N. Siddiquee, Microstructure, mechanical properties and electrochemical behavior of a novel biomedical titanium alloy subjected to thermo-mechanical processing including aging, *J. Alloys Compd.* 634 (2015) 272–280. [doi:10.1016/j.jallcom.2015.02.095](https://doi.org/10.1016/j.jallcom.2015.02.095)
- [30] S. Bahl, S. Das, S. Suwas, K. Chatterjee, Engineering the next-generation tin containing  $\beta$  titanium alloys with high strength and low modulus for orthopedic applications, *J. Mech. Behav. Biomed. Mater.* 78 (2018) 124–133. [doi:10.1016/j.jmbbm.2017.11.014](https://doi.org/10.1016/j.jmbbm.2017.11.014)
- [31] J. Cheng, J. Li, S. Yu, Z. Du, X. Zhang, W. Zhang, J. Gai, H. Wang, H. Song, Z. Yu, Influence of isothermal  $\omega$  transitional phase assisted phase transition from  $\beta$  to  $\alpha$  on room-temperature mechanical performance of a metastable  $\beta$  titanium alloy Ti-10Mo-6Zr-4Sn-3Nb (Ti-B12) for medical application, *Front. Bioeng. Biotechnol.* 8 (2021) 1518. [doi:10.3389/fbioe.2020.626665](https://doi.org/10.3389/fbioe.2020.626665)
- [32] J. Cheng, J. Li, S. Yu, Z. Du, X. Zhang, W. Zhang, J. Gai, H. Wang, H. Song, Z. Yu, Cold rolling deformation characteristic of a biomedical beta type Ti-25Nb-3Zr-2Sn-3Mo alloy plate and its influence on  $\alpha$  precipitated phases and room temperature mechanical properties during aging treatment, *Front. Bioeng. Biotechnol.* 8 (2020) 598529. [doi:10.3389/fbioe.2020.598529](https://doi.org/10.3389/fbioe.2020.598529)
- [33] Z. Du, H. Guo, J. Liu, J. Cheng, X. Zhao, X. Wang, F. Liu, X. Cui, Microstructure evolution during aging heat treatment and its effects on tensile properties and dynamic Young's modulus of a biomedical  $\beta$  titanium alloy, *Mater. Sci. Eng. A* 791 (2020) 139677. [doi:10.1016/j.msea.2020.139677](https://doi.org/10.1016/j.msea.2020.139677)
- [34] I. Weiss, S. L. Semiatin, Thermomechanical processing of beta titanium alloys – an overview, *Mater. Sci. Eng. A* 243 (1998) 46–65. [doi:10.1016/S0921-5093\(97\)00783-1](https://doi.org/10.1016/S0921-5093(97)00783-1)
- [35] M. J. Torkamany, F. Malek Ghaini, R. Poursalehi, An insight to the mechanism of weld penetration in dissimilar pulsed laser welding of niobium and Ti-6Al-4V, *Opt. Laser Technol.* 79 (2016) 100–107. [doi:10.1016/j.optlastec.2015.11.005](https://doi.org/10.1016/j.optlastec.2015.11.005)
- [36] K. Norrish, R. M. Taylor, Quantitative analysis by X-ray diffraction, *Clay Miner. Bull.* 5 (1962) 98–109. [doi:10.1180/claymin.1962.005.28.06](https://doi.org/10.1180/claymin.1962.005.28.06)
- [37] K. K. Wong, H. C. Hsu, S. C. Wu, W. F. Ho, Structure and properties of Ti-rich Ti-Zr-Nb-Mo medium-entropy alloys, *J. Alloys Compd.* 868 (2021) 159137. [doi:10.1016/j.jallcom.2021.159137](https://doi.org/10.1016/j.jallcom.2021.159137)
- [38] T. Kokubo, H. Takadama, How useful is SBF in predicting in vivo bone bioactivity? *Biomaterials* 27 (2006) 2907–2915. [doi:10.1016/j.biomaterials.2006.01.017](https://doi.org/10.1016/j.biomaterials.2006.01.017)
- [39] J. Cheng, J. Li, S. Yu, Z. Du, F. Dong, J. Zhang, X. Zhang, Corrosion behavior of as-cast Ti-10Mo-6Zr-4Sn-3Nb and Ti-6Al-4V in Hank's solution: a comparison investigation, *Metals* 11 (2021) 11. [doi:10.3390/met11010011](https://doi.org/10.3390/met11010011)
- [40] M. J. Lai, C. C. Tasan, J. Zhang, B. Grabowski, L. F. Huang, D. Raabe, Origin of shear induced  $\beta$  to  $\omega$  transition in Ti-Nb-based alloys, *Acta Mater.* 92 (2015) 55–63. [doi:10.1016/j.actamat.2015.03.040](https://doi.org/10.1016/j.actamat.2015.03.040)
- [41] H. Liu, M. Niinomi, M. Nakai, K. Cho, Athermal and deformation-induced  $\omega$ -phase transformations in biomedical beta-type alloy Ti-9Cr-0.2O, *Acta Mater.* 106 (2016) 162–170. [doi:10.1016/j.actamat.2016.01.008](https://doi.org/10.1016/j.actamat.2016.01.008)
- [42] H. Liu, M. Niinomi, M. Nakai, K. Cho, H. Fujii, Deformation-induced  $\omega$ -phase transformation in a  $\beta$ -type titanium alloy during tensile deformation, *Scripta Mater.* 130 (2017) 27–31. [doi:10.1016/j.scriptamat.2016.10.036](https://doi.org/10.1016/j.scriptamat.2016.10.036)
- [43] W. Chen, K. Li, G. Yu, J. Ren, Y. Zha, J. Sun, Deformation twinning-induced single-variant  $\omega$ -plates in metastable  $\beta$ -Ti alloys containing athermal  $\omega$ -precipitates, *J. Mater. Sci.* 56 (2021) 7710–7726. [doi:10.1007/s10853-020-05706-z](https://doi.org/10.1007/s10853-020-05706-z)
- [44] Q. Meng, S. Guo, Q. Liu, L. Hu, X. Q. Zhao, A  $\beta$ -type TiNbZr alloy with low modulus and high strength for biomedical applications, *Prog. Nat. Sci.: Mater. Int.* 24 (2014) 157–162. [doi:10.1016/j.pnsc.2014.03.007](https://doi.org/10.1016/j.pnsc.2014.03.007)
- [45] Y. Mantani, M. Tajima, Phase transformation of quenched  $\alpha''$  martensite by aging in Ti-Nb alloys, *Mater. Sci. Eng. A* 438–440 (2006) 315–319. [doi:10.1016/j.msea.2006.02.180](https://doi.org/10.1016/j.msea.2006.02.180)
- [46] W. F. Cui, A. H. Guo, Microstructures and properties of biomedical TiNbZrFe  $\beta$ -titanium alloy under aging conditions, *Mater. Sci. Eng. A* 527 (2009) 258–262. [doi:10.1016/j.msea.2009.08.057](https://doi.org/10.1016/j.msea.2009.08.057)
- [47] Q. Meng, Q. Liu, S. Guo, Y. Zhu, X. Zha, Effect of thermo-mechanical treatment on mechanical and elastic properties of Ti-36Nb-5Zr alloy, *Prog. Nat. Sci.* 25 (2015) 229–235. [doi:10.1016/j.pnsc.2015.05.001](https://doi.org/10.1016/j.pnsc.2015.05.001)
- [48] R. Santhosh, M. Geetha, M. Nageswara Rao, Recent developments in heat treatment of beta titanium alloys for aerospace applications, *Trans. Indian Inst. Met.* 70 (2017) 1681–1688. [doi:10.1007/s12666-016-0985-6](https://doi.org/10.1007/s12666-016-0985-6)
- [49] R. P. Kolli, A. Devaraj, A review of metastable beta titanium alloys, *Metals* 8 (2018) 506. [doi:10.3390/met8070506](https://doi.org/10.3390/met8070506)
- [50] J. Vishnu, M. Sankar, H. J. Rack, N. Rao, A. K. Singh, G. Manivasagam, Effect of phase transformations during aging on tensile strength and ductility of metastable  $\beta$  titanium alloy Ti-35Nb-7Zr-5Ta-0.35O for orthopedic applications, *Mater. Sci. Eng. A* 779 (2020) 139127. [doi:10.1016/j.msea.2020.139127](https://doi.org/10.1016/j.msea.2020.139127)
- [51] S. V. Santos, G. D. Lima, B. L. Nascimento, L. S. Fontes, S. Griza, The effect of cold working and solution heat treatment on microstructure and mechanical behavior of Ti35Nb2.5Sn alloy, *Tecnol. Metal. Mater. Min.* 18 (2021) e2453. [doi:10.4322/2176-1523.20202453](https://doi.org/10.4322/2176-1523.20202453)

- [52] J. Cheng, H. Wang, J. Li, J. Gai, J. Ru, Z. Du, J. Fan, J. Niu, H. Song, Z. Yu, The effect of cold swaging deformation on the microstructures and mechanical properties of a novel metastable  $\beta$  type Ti-10Mo-6Zr-4Sn-3Nb alloy for biomedical devices, *Front. Mater.* 7 (2020) 228. [doi:10.3389/fmats.2020.00228](https://doi.org/10.3389/fmats.2020.00228)
- [53] S. J. Li, M. Niinomi, T. Akahori, T. Kasuga, R. Yang, Y. L. Hao, Fatigue characteristics of bioactive glass-ceramic-coated Ti-29Nb-13Ta-4.6Zr for biomedical application, *Biomaterials* 25 (2004) 3369–3378. [doi:10.1016/j.biomaterials.2003.09.108](https://doi.org/10.1016/j.biomaterials.2003.09.108)
- [54] J. Hernandez, S. J. Li, E. Martinez, L. E. Murr, X. M. Pan, K. N. Amato, X. Y. Cheng, F. Yang, C. A. Terrazas, S. M. Gaytan, Y. L. Hao, R. Yang, F. Medina, R. B. Wicker, Microstructures and hardness properties for  $\beta$ -phase Ti-24Nb-4Zr-7.9Sn alloy fabricated by electron beam melting, *J. Mater. Sci.* 29 (2013) 1011–1017. [doi:10.1016/j.jmst.2013.08.023](https://doi.org/10.1016/j.jmst.2013.08.023)
- [55] E. Ghassemali, R. Sonkusare, K. Biswas, N. P. Gurao, In-situ study of crack initiation and propagation in a dual phase AlCoCrFeNi high entropy alloy, *J. Alloys Compd.* 710 (2017) 539–546. [doi:10.1016/j.jallcom.2017.03.307](https://doi.org/10.1016/j.jallcom.2017.03.307)
- [56] Q. Wang, Y. Lu, Q. Yu, Z. Zhang, The exceptional strong face-centered cubic phase and semi-coherent phase boundary in a eutectic dual-phase high entropy alloy AlCoCrFeNi, *Sci. Rep.* 8 (2018) 14910. [doi:10.1038/s41598-018-33330-0](https://doi.org/10.1038/s41598-018-33330-0)
- [57] B. Ellyson, J. Klemm-Toole, K. Clarke, R. Field, M. Kaufman, A. Clarke, Tuning the strength and ductility balance of a TRIP titanium alloy, *Scripta Mater.* 194 (2021) 113641. [doi:10.1016/j.scriptamat.2020.113641](https://doi.org/10.1016/j.scriptamat.2020.113641)
- [58] W. Wang, X. Zhang, W. Mei, J. Sun, Role of omega phase evolution in plastic deformation of twinning-induced plasticity  $\beta$  Ti-12V-2Fe-1Al alloy, *Mater. Des.* 186 (2020) 108282. [doi:10.1016/j.matdes.2019.108282](https://doi.org/10.1016/j.matdes.2019.108282)
- [59] W. Zhang, K. Fang, Y. Hu, S. Wang, X. Wang, Effect of machining-induced surface residual stress on initiation of stress corrosion cracking in 316 austenitic stainless steel, *Corros. Sci.* 108 (2016) 173–184. [doi:10.1016/j.corsci.2016.03.008](https://doi.org/10.1016/j.corsci.2016.03.008)